nature physics

LETTERS

PUBLISHED ONLINE: 5 JUNE 2011 | DOI: 10.1038/NPHYS2010

The pirouette effect in turbulent flows

Haitao Xu[1], Alain Pumir[2] and Eberhard Bodenschatz[1,3,4]*

The disorganized fluctuations of turbulence are crucial in the transport of particles or chemicals[1,2] and could play a decisive role in the formation of rain in clouds[3], the accretion process in protoplanetary disks[4], and how animals find their mates or prey[5,6]. These and other examples[7] suggest a yet-to-be-determined unifying structure of turbulent flows[8,9]. Here, we unveil an important ingredient of turbulence by taking the perspective of an observer who perceives its world with respect to three distant neighbours all swept by the flow. The time evolution of the observer's world can be decomposed into rotation and stretching. We show that, in this Lagrangian frame, the axis of rotation aligns with the initially strongest stretching direction, and that the dynamics can be understood by the conservation of angular momentum. This 'pirouette effect' thus appears as an important structural component of turbulence, and elucidates the mechanism for small-scale generation in turbulence.

To an observer who perceives its world with respect to three distant fluid tracers, all carried by the flow, the seemingly random turbulent motion modifies the distances to and between them. Turbulent motion, on average, separates two tracers[10–12]. However, as shown in Fig. 1, given a set of four tracers initially located on a regular tetrahedron, that is, with all pairs equally separated by a distance R_0, the growth of the distance between pairs is very uneven, resulting in strong shape deformation[13–16]. As first observed in ref. 17, the resulting 'minimal' four-point description provides important insights into the dynamics of turbulence.

Remarkably, our study of the relative motion between these neighbouring particles, as shown in Fig. 1, reveals the alignment of the rotation towards the direction of the initially strongest stretching, while the angular momentum remains constant (statistically, see Supplementary Information). This is a manifestation of the 'pirouette effect', well known from classical ballet or ice-skating.

We used a particle tracking technique to follow several hundreds of nearly neutrally buoyant, 30 μm size polystyrene particles as tracers in a turbulent water flow[11,18,19] with high turbulence intensities as defined by the Taylor microscale Reynolds number[10,20] $350 \leq R_\lambda \leq 815$. We recorded tracer motion in volumes as large as $(5\,\mathrm{cm})^3$ with a spatial resolution of approximately 20 μm and a time resolution of 0.04 ms by stereoscopic observation using three high-speed cameras. We accurately determined the trajectories and velocities of millions of tracers in three dimensions, from which we extracted the dynamics of initially regular tetrahedra by conditioning statistics on four tracers with nearly equal mutual distances (as in ref. 15 and Supplementary Information). We complemented the experiments by direct numerical simulations (DNS) of the Navier–Stokes equations for $100 \leq R_\lambda \leq 170$ (ref. 14).

The time evolution of the observer's world can be decomposed into rotation and stretching, which is measured by the perceived velocity gradient $\mathbf{M}$, defined as:

$$u_i^a = \rho_j^a M_{ji} \tag{1}$$

where ρ_i^a and u_i^a represent the component in the direction i ($i = 1, 2$ or 3) of the position and velocity of the ath tracer (see Supplementary Information). The perceived velocity gradient, $\mathbf{M}$, can then be uniquely decomposed as a sum of a straining motion, $\mathbf{S}$, and of a rotation, $\mathbf{\Omega}$: $\mathbf{M} = \mathbf{S} + \mathbf{\Omega}$, with $\mathbf{S} \equiv (\mathbf{M} + \mathbf{M}^T)/2$ and $\mathbf{\Omega} \equiv (\mathbf{M} - \mathbf{M}^T)/2$. In addition, the straining motion can be understood as a superposition of simple stretching or compression along three orthogonal directions, denoted $\hat{\mathbf{e}}_i$. The corresponding three stretching rates λ_i are arranged here in decreasing order: $\lambda_1 \geq \lambda_2 \geq \lambda_3$. A positive (respectively negative) value of λ_i corresponds to stretching (respectively compression) along the direction given by $\hat{\mathbf{e}}_i$. The rotation matrix $\mathbf{\Omega}$ is 'characterized' by a local rotation vector $\boldsymbol{\omega}$ with its direction denoted as $\hat{\mathbf{e}}_\omega$ (note that the conventional vorticity vector is $2\boldsymbol{\omega}$). The angular momentum of the system of four points, $\mathbf{\Gamma}$, defined by:

$$\mathbf{\Gamma} = \sum_{a=1}^{3} \rho^a \times \mathbf{u}^a \tag{2}$$

is related, to a good approximation (see Supplementary Information), to the rotation vector through the relation $\mathbf{\Gamma} = \mathbf{I} \cdot \boldsymbol{\omega}$, where $\mathbf{I}$ is the moment of inertia tensor familiar in classical mechanics[21]. In qualitative terms, the angular momentum $\mathbf{\Gamma}$ is proportional to the rotation vector $\boldsymbol{\omega}$, multiplied by the square of a distance, which characterizes the extent of the set of points in the direction transverse to the direction of rotation vector $\boldsymbol{\omega}$. For a Lagrangian tetrahedron, angular momentum is not strictly conserved (as studied in the Supplementary Information). However, as we demonstrate below, the conservation is a good approximation for the short times we examined.

The shape dynamics can be conveniently studied in the basis given by the eigenvectors $(\hat{\mathbf{e}}_1(0), \hat{\mathbf{e}}_2(0), \hat{\mathbf{e}}_3(0))$ of the strain at a chosen initial time at which the tetrads are equilateral. The strong stretching in the direction $\hat{\mathbf{e}}_1(0)$ results in the shape becoming thinner in the direction 1, thus leading to a reduction of the component $\mathbf{I}_{11}$, compared to the components in the other directions $\mathbf{I}_{22}$ and $\mathbf{I}_{33}$. If angular momentum is conserved, then it implies that the direction of rotation $\hat{\mathbf{e}}_\omega$ at a time $t + \Delta t$ should align preferentially with the initial stretching direction $\hat{\mathbf{e}}_1(0)$. The effect is clearly demonstrated in our experiments, as shown in Fig. 2.

The time evolution of the alignment between the initial stretching $\hat{\mathbf{e}}_i(0)$ and rotation $\hat{\mathbf{e}}_\omega(t)$ can be quantified by studying the square of the cosine of the angles between the unit vectors:

$$C_{i,\omega}(t) \equiv \langle (\hat{\mathbf{e}}_i(0) \cdot \hat{\mathbf{e}}_\omega(t))^2 \rangle$$

[1]Laboratory for Fluid Dynamics, Pattern-Formation and Nanobiocomplexity, Max Planck Institute for Dynamics and Self-Organisation, Am Fassberg 17, Göttingen, D-37077, Germany, [2]Laboratoire de Physique, Ecole Normale Supérieure de Lyon, Université Lyon 1 and CNRS, F-69007 Lyon, France, [3]Institute for Nonlinear Dynamics, University of Göttingen, D-37077, Germany, [4]Laboratory of Atomic and Solid State Physics and Sibley School of Mechanical and Aerospace Engineering, Cornell University, Ithaca, New York 14853, USA. *e-mail: ebodens@gwdg.de.

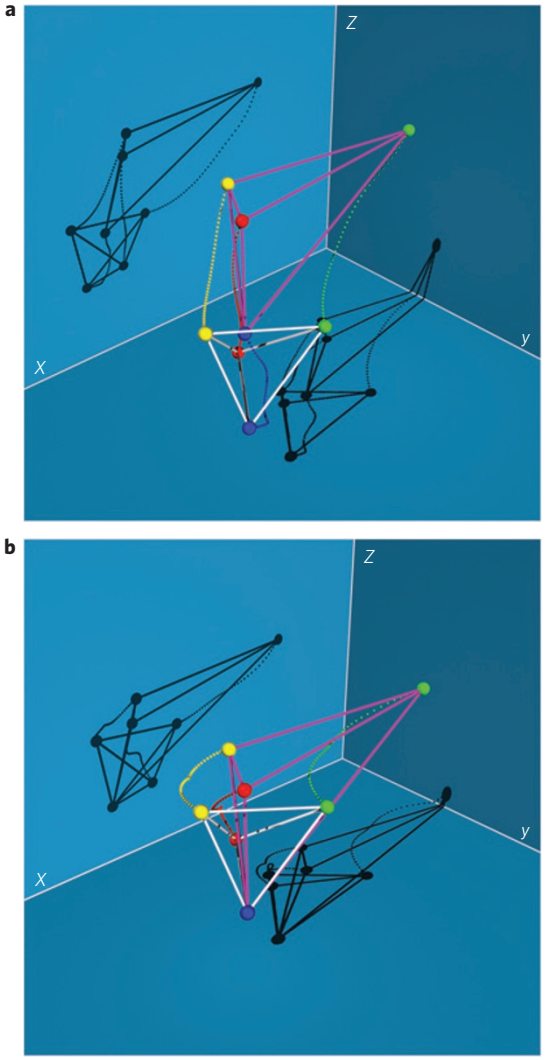

Figure 1 | Tetrahedron shape deformation by turbulent flows. a, Four tracers, defining initially the regular tetrahedron with white edges, initially of size R_0, evolved into the deformed tetrahedron with purple edges. The dotted lines mark the trajectories of each of the tracers. **b**, The motion of the tetrahedron's vertices, as seen by the blue 'observer', leads to an elongation of the shape in a particular direction. The experimental data was obtained in a turbulent flow at $R_\lambda = 350$. The initial size of the tetrahedron's edges is $R_0 = 8$ mm. The size of the largest whirls of the flow (the integral length scale) is $L = 70$ mm; the size of the smallest whirls (the Kolmogorov scale) is $\eta = 84\,\mu$m. The time separating the initial (white) and final (purple) tetrahedron is $t = 56$ ms, which corresponds to $0.4t_0$ (t_0 defined in the text) for this tetrahedron. The dots along the trajectories indicate the locations of the vertices at time intervals of $\Delta t = 2$ ms. The size of the tetrads remains within the inertial range during the time interval discussed here ($t \leq 0.4t_0$), see Supplementary Information.

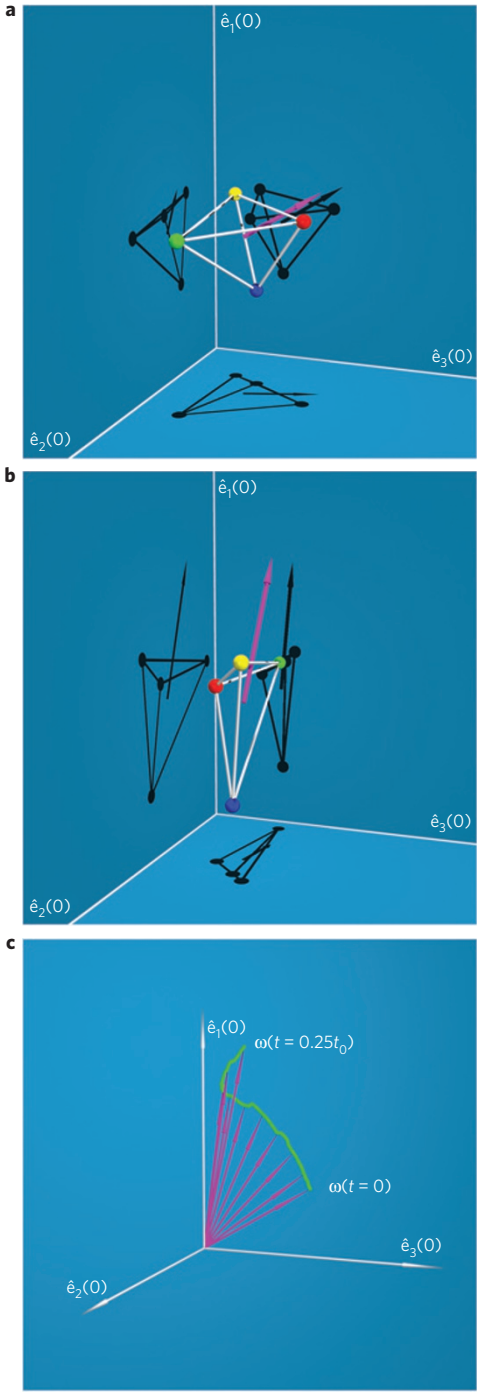

Figure 2 | The Pirouette effect: alignment of the rotation vector with the direction of the initially strongest stretching. a, The initial shape of the tetrahedron and the rotation vector, $\boldsymbol{\omega}$ (purple arrow), shown in the reference frame specified by the eigenvectors ($\hat{\mathbf{e}}_1(0), \hat{\mathbf{e}}_2(0), \hat{\mathbf{e}}_3(0)$) of the strain. The direction associated with the fastest stretching, $\hat{\mathbf{e}}_1(0)$, is vertical. **b**, The tetrahedron, shown at $t = 36$ ms, or $0.25t_0$, has elongated in the vertical direction $\hat{\mathbf{e}}_1(0)$. This elongation results in a reduced moment of inertia in the $\hat{\mathbf{e}}_1(0)$ direction, compared with the two other directions. **c**, The rotation vector $\boldsymbol{\omega}(t)$ aligns with the initial direction of the fastest stretching $\hat{\mathbf{e}}_1(0)$. This is consistent with angular momentum conservation. The example shown here is the same tetrahedron as in Fig. 1.

where the brackets $\langle\cdot\rangle$ denote an average over many configurations, starting with an initially regular tetrahedron of fixed size. As a point of reference, we note that when the two vectors $\hat{\mathbf{e}}_i$ and $\hat{\mathbf{e}}_\omega$ are randomly oriented with respect to each other, the distribution of $|\hat{\mathbf{e}}_i \cdot \hat{\mathbf{e}}_\omega|$ is uniform, and the value of $\langle(\hat{\mathbf{e}}_i \cdot \hat{\mathbf{e}}_\omega)^2\rangle$ is equal to 1/3. A value of $\langle(\hat{\mathbf{e}}_i \cdot \hat{\mathbf{e}}_\omega)^2\rangle$ greater or less than 1/3 indicates that the two vectors tend to be oriented preferentially parallel or perpendicular to each other.

Figure 3 quantifies the alignment effect between the direction of the rotation vector $\hat{\mathbf{e}}_\omega(t)$ with the strongest initial stretching direction $\hat{\mathbf{e}}_1(0)$ for different turbulence levels and regular tetrahedra with side length R_0. The distances R_0 were chosen in the inertial range, where neither the viscosity nor the large-scale details of the flow are expected to play a role[20]. As shown in Fig. 3a, the function

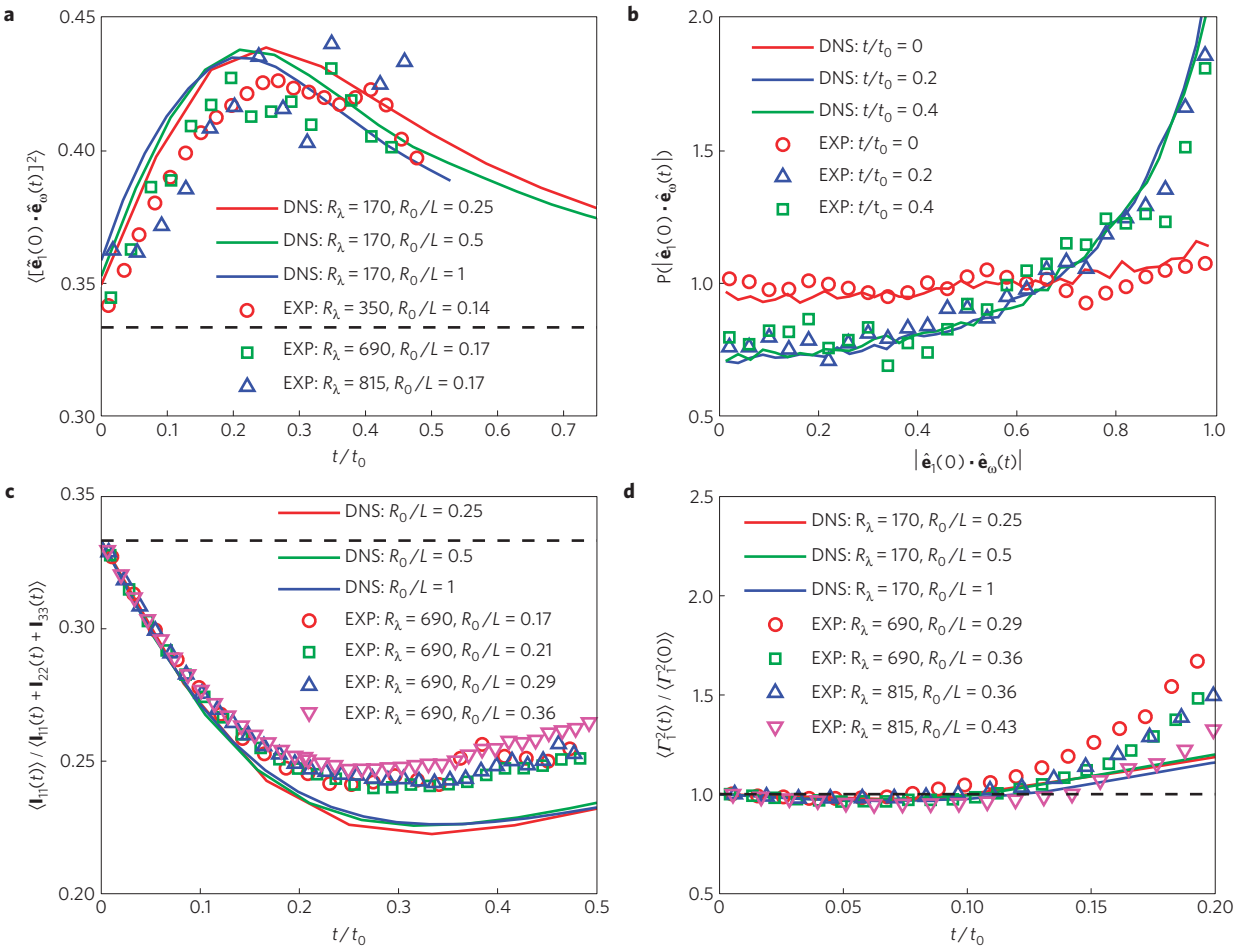

Figure 3 | Alignment of $\hat{\mathbf{e}}_\omega(t)$ with $\hat{\mathbf{e}}_1(0)$ for tetrahedra with different initial sizes R_0 and flows with different turbulence levels, as indicated by the Reynolds number R_λ. a, The evolution of $C_{1,\omega}(t)$, measuring the alignment of $\hat{\mathbf{e}}_\omega(t)$ and $\hat{\mathbf{e}}_1(0)$, as a function of t/t_0, with $t_0=(R_0^2/\varepsilon)^{1/3}$. At $t=0$, $C_{1,\omega}$ is very close to 1/3, implying a nearly random alignment between $\hat{\mathbf{e}}_1(0)$ and $\hat{\mathbf{e}}_\omega(0)$. The increase of $C_{1,\omega}(t)$ indicates that the direction of rotation $\hat{\mathbf{e}}_\omega(t)$ becomes aligned with $\hat{\mathbf{e}}_1(0)$ during the early stage of the evolution. The maximum of $C_{1,\omega}(t)$ is reached at $t_{\max}\sim 0.25t_0$. Data from experiments (labelled as EXP) are shown as symbols and the numerical results (labelled as DNS) are shown as solid lines. **b**, The evolution of the PDF of the cosine of the angle between $\hat{\mathbf{e}}_\omega(t)$ and $\hat{\mathbf{e}}_1(0)$, for tetrahedra with an initial size $R_0=15$ mm, corresponding to $R_0/\eta=500$ or $R_0/L=0.21$, in an intense turbulent flow with Reynolds number $R_\lambda=690$. At times $0.2\le t/t_0\le 0.4$, the PDFs peak at values of the cosine close to 1, that is, nearly complete alignment between the two vectors. **c**, The evolution of the relative value of the moment of inertia tensor in the direction of $\hat{\mathbf{e}}_1(0)$: $\langle \mathbf{I}_{11}(t)\rangle/\langle \mathbf{I}_{11}(t)+\mathbf{I}_{22}(t)+\mathbf{I}_{33}(t)\rangle$. The decrease of the moment of inertia tensor in this direction is a consequence of the strong stretching along $\hat{\mathbf{e}}_1(0)$. The minimum value of $\langle \mathbf{I}_{11}(t)\rangle/\langle \mathbf{I}_{11}(t)+\mathbf{I}_{22}(t)+\mathbf{I}_{33}(t)\rangle$ is reached at the time where the alignment between $\hat{\mathbf{e}}_\omega(t)$ and $\hat{\mathbf{e}}_1(0)$ is the most significant. **d**, Conservation of angular momentum along $\hat{\mathbf{e}}_1(0)$, as measured by the change of the angular momentum $\Gamma_1^2(t)$ relative to its initial value $\Gamma_1^2(0)$. In all the experimental data, the initial size of the tetrahedra R_0 are within the inertial range ($\eta\ll R_0<L$). At $R_\lambda=350$, 690 and 815, the corresponding ratios between the integral scale and the Kolmogorov scale are, respectively, $L/\eta\approx 830$, 2,300, and 3,000.

$C_{1,\omega}(t)$ starts at a value very close to 1/3 at time $t=0$, indicating little correlation between the two vectors at time $t=0$. Then the function $C_{1,\omega}(t)$ increases significantly with time, to a value of approximately 0.45 at a time $t\approx 0.2t_0$, where $t_0=(R_0^2/\varepsilon)^{1/3}$ is the characteristic turbulent time at scale R_0 for a flow with energy dissipation rate per unit mass ε in the classical Kolmogorov theory[20]. As shown in Fig. 3b, at $t\approx t_0/4$ and $t_0/2$ the probability density functions (PDFs) of $|\hat{\mathbf{e}}_1(0)\cdot\hat{\mathbf{e}}_\omega(t)|$ peaks at $|\hat{\mathbf{e}}_1(0)\cdot\hat{\mathbf{e}}_\omega(t)|\approx 1$, whereas at $t\approx 0$ it is flat. This demonstrates beautifully the preferential alignment between the two vectors for $t>0$. The origin of the alignment can be traced to the weakening of the component of the moment of inertia tensor matrix $\mathbf{I}_{11}$, due to the strong stretching along the direction $\hat{\mathbf{e}}_1(0)$ compared with the two other components $\mathbf{I}_{22}$ and $\mathbf{I}_{33}$. Remarkably, the relative value of $\mathbf{I}_{11}$ reaches a minimum at $t_{\max}\approx 0.2-0.3t_0$ (Fig. 3c). This is the time needed to reach the best alignment between rotation and the strongest initial stretching direction $\hat{\mathbf{e}}_1(0)$. This is expected from angular momentum conservation. Figure 3d demonstrates that for short times, up to $0.1t_0$, angular momentum is conserved. The mean value of $\Gamma_1^2(t)$, divided by its initial value at $t=0$, is shown as a function of t/t_0 for several initial sizes R_0. A slow increase of $\mathbf{I}_{11}(t)$, induced by the increase in inter-particle separation at later time (relative turbulent dispersion[9–12]), caused the observed drift in $\Gamma_1^2(t)$. Our results thus suggest that, in the inertial range, the dynamics of alignment is statistically self-similar, and depends simply on time and initial scales through the reduced variable t/t_0. In addition, our numerical simulations show that the alignment of the vectors $\hat{\mathbf{e}}_1(0)$ and $\hat{\mathbf{e}}_\omega(t)$ is observed even at smaller scales, where viscosity dominates, albeit with a viscous timescale.

The alignment properties between the rotation direction $\hat{\mathbf{e}}_\omega$ and the stretching direction $\hat{\mathbf{e}}_i$ at the same time have been investigated for the true velocity gradient tensor[22–29]. On the basis of the intuitive notion that stretching is strongest in the direction $\hat{\mathbf{e}}_1$, it was expected that there would be a strong alignment of $\hat{\mathbf{e}}_\omega$ with $\hat{\mathbf{e}}_1$. In contrast, it was found that the direction $\hat{\mathbf{e}}_\omega$ is essentially

independent of the equal-time strongest stretching $\hat{\mathbf{e}}_1$, but rather aligns preferentially with the direction of the intermediate rate of strain, $\hat{\mathbf{e}}_2$, which is associated on average with weaker stretching[22,23]. This misalignment between $\hat{\mathbf{e}}_1$ and $\hat{\mathbf{e}}_\omega$ weakens the nonlinear interaction between strain and rotation that is known to be necessary for the generation of smaller scales from larger ones, which is the hallmark of turbulence[10]. This puzzling observation has since been the subject of numerous studies[24–27,29].

Our results shed new light on this puzzle. The strain does indeed align rotation $\hat{\mathbf{e}}_\omega(t)$ with the strongest initial stretching direction $\hat{\mathbf{e}}_1(0)$, albeit with a spatial-scale dependent delay of $\sim 0.2 - 0.3t_0$. Our DNS results show this conclusion to extend down to the Kolmogorov scale, where $\mathbf{M}$ reduces to the true velocity gradient tensor. Thus, the alignment with the initially strongest stretching direction is a dynamical process: not surprisingly, the alignment between $\hat{\mathbf{e}}_\omega(t)$ and $\hat{\mathbf{e}}_1(0)$ builds up over time. Understanding the alignment properties between $\hat{\mathbf{e}}_\omega$ and the eigenvectors of the strain $\hat{\mathbf{e}}_1$ at equal time (Eulerian point of view) requires a proper description of the rotation of the eigenvectors $(\hat{\mathbf{e}}_1(t), \hat{\mathbf{e}}_2(t), \hat{\mathbf{e}}_3(t))$, which is affected by nonlocal (pressure) effects[28]. The time of decorrelation between the direction of $\hat{\mathbf{e}}_1(t)$ and $\hat{\mathbf{e}}_1(0)$ is found to be on the order of $0.2t_0$, comparable to the time of alignment of $\hat{\mathbf{e}}_\omega(t)$ and $\hat{\mathbf{e}}_1(0)$, thus explaining the lack of observed alignment between $\hat{\mathbf{e}}_\omega(t)$ and $\hat{\mathbf{e}}_1(t)$. Our numerical data demonstrates that the much-reduced picture discussed extends to the true velocity gradient tensor and thus adequately captures the physics of turbulent small scale generation[17,30].

Received 1 January 2011; accepted 4 May 2011; published online 5 June 2011

References

1. Mafra-Neto, A. & Cardé, R. T. Fine-scale structure of pheromone plumes modulates upwind orientation of flying moths. *Nature* **369,** 142–144 (1994).
2. Abraham, E. R. *et al.* Importance of stirring in the development of an iron-fertilized phytoplankton bloom. *Nature* **407,** 727–730 (2000).
3. Bodenschatz, E., Malinowski, S. P., Shaw, R. A. & Stratmann, F. Can we understand clouds without turbulence? *Science* **327,** 970–971 (2010).
4. Johansen, A. *et al.* Rapid planetesimal formation in turbulent circumstellar disks. *Nature* **448,** 1022–1025 (2007).
5. Ferner, M. C. & Weissburg, M. J. Slow-moving predatory gastropods track prey odors in fast and turbulent flow. *J. Exp. Biol.* **208,** 809–819 (2005).
6. Vergassola, M., Villermaux, E. & Shraiman, B. I. 'Infotaxis' as a strategy for searching without gradients. *Nature* **445,** 406–409 (2007).
7. Corrsin, S. Turbulence. *Am. Scient.* **49,** 300–325 (1961).
8. Shraiman, B. I. & Siggia, E. D. Scalar turbulence. *Nature* **405,** 639–646 (2000).
9. Falkovich, G., Gawedzki, K. & Vergassola, M. Particles and fields in fluid turbulence. *Rev. Mod. Phys.* **73,** 913–975 (2001).
10. Tennekes, H. & Lumley, J. L. *A First Course in Turbulence* (MIT Press, 1970).
11. Bourgoin, M. *et al.* The role of pair dispersion in turbulent flow. *Science* **311,** 835–838 (2006).
12. Salazar, J. P. L. C & Collins, L. R. Two-particle dispersion in isotropic turbulent flows. *Annu. Rev. Fluid Mech.* **41,** 405–432 (2009).
13. Girimaji, S. S. & Pope, S. B. Material-element deformation in isotropic turbulence. *J. Fluid Mech.* **220,** 427–458 (1990).
14. Pumir, A., Shraiman, B. I. & Chertkov, M. Geometry of Lagrangian dispersion in turbulence. *Phys. Rev. Lett.* **85,** 5324–5327 (2000).
15. Xu, H., Ouellette, N. T. & Bodenschatz, E. Evolution of geometric structures in intense turbulence. *New J. Phys.* **10,** 013012 (2008).
16. Toschi, F. & Bodenschatz, E. Lagrangian properties of particles in turbulence. *Annu. Rev. Fluid Mech.* **41,** 375–404 (2009).
17. Chertkov, M., Pumir, A. & Shraiman, B. I. Lagrangian tetrad dynamics and the phenomenology of turbulence. *Phys. Fluids* **11,** 2394–2410 (1999).
18. Ouellette, N. T., Xu, H. & Bodenschatz, E. A quantitative study of three-dimensional Lagrangian particle tracking algorithms. *Exp. Fluids* **40,** 301–313 (2006).
19. Xu, H. Tracking Lagrangian trajectories in position-velocity space. *Meas. Sci. Technol.* **19,** 075105 (2008).
20. Frisch, U. *Turbulence: The Legacy of A. N. Kolmogorov* (Cambridge Univ. Press, 1995).
21. Goldstein, H. *Classical Mechanics* (Addison Wesley, 1960).
22. Siggia, E. D. Invariants for the one-point vorticity and strain rate correlation functions. *Phys. Fluids* **24,** 1934–1936 (1981).
23. Ashurst, W. T., Kerstein, A. R., Kerr, R. M. & Gibson, C. H. Alignment of vorticity and scalar gradient with strain rate in simulated Navier–Stokes turbulence. *Phys. Fluids* **30,** 2343–2353 (1987).
24. She, Z. S., Jackson, E. & Orszag, S. A. Structure and dynamics of homogeneous turbulence: Models and simulations. *Proc. R. Soc. Lond. A* **434,** 101–124 (1991).
25. Tsinober, A., Kit, E. & Dracos, T. Experimental investigation of the field of velocity gradients in turbulent flows. *J. Fluid Mech.* **242,** 169–192 (1992).
26. Zeff, B. W. *et al.* Measuring intense rotation and dissipation in turbulent flows. *Nature* **421,** 146–149 (2003).
27. Lüthi, B., Tsinober, A. & Kinzelbach, W. Lagrangian measurement of vorticity dynamics in turbulent flows. *J. Fluid Mech.* **528,** 87–118 (2005).
28. Hamlington, P. E., Schumacher, J. & Dahm, W. J. A. Direct assessment of vorticity alignment with local and non local strain rates in turbulent flows. *Phys. Fluids* **20,** 111703 (2008).
29. Wallace, J. M. Twenty years of experimental and direct numerical simulation access to the velocity gradient tensor: What have we learned about turbulence? *Phys. Fluids* **21,** 021301 (2009).
30. Pumir, A., Shraiman, B. I. & Chertkov, M. The Lagrangian view of energy transfer in turbulent flow. *Eur. Phys. Lett.* **56,** 379–385 (2001).

Acknowledgements

We are grateful to B. Shraiman and E. Siggia for discussions. A.P. thanks IDRIS for providing the computation resources and the ANR for financial support through the contract DSPET. E.B. and H.X. thank the Max Planck Society for support. This research was supported in part by the US National Science Foundation under Grant No. NSF PHY05-51164 and the European COST Action MP0806.

Author contributions

H.X. and E.B. designed and performed the experiments. H.X. and E.B. analysed the experimental data. A.P. conducted the numerical simulations and analyzed the numerical data. All authors discussed the physics and wrote the manuscript.

Additional information

The authors declare no competing financial interests. Supplementary information accompanies this paper on www.nature.com/naturephysics. Reprints and permissions information is available online at http://www.nature.com/reprints. Correspondence and requests for materials should be addressed to E.B.